A model of task-level human stepping regulation yields semistable walking

Navendu S. Patil[1,2], Jonathan B. Dingwell[1] and Joseph P. Cusumano[2*]

[1]Department of Kinesiology, and [2]Department of Engineering Science & Mechanics, Pennsylvania State University, University Park, PA 16802, USA

March 5, 2024

Abstract

A simple lateral dynamic walker, with swing leg dynamics and three adjustable input parameters, is used to study how motor regulation affects frontal plane stepping. Motivated by experimental observations and phenomenological models, we imposed task-level multiobjective regulation targeting the walker's optimal lateral foot placement at each step. The regulator prioritizes achieving step width and lateral body position goals to varying degrees by choosing a mixture parameter. Our model thus integrates a lateral *mechanical template*, which captures fundamental mechanics of frontal-plane walking, with a lateral *motor regulation template*, an empirically verified model of how humans manipulate lateral foot placements in a goal-directed manner. The model captures experimentally observed stepping fluctuation statistics and demonstrates how linear empirical models of stepping dynamics can emerge from first-principles nonlinear mechanics. We find that task-level regulation gives rise to a goal equivalent manifold in the system's extended state space of mechanical states and inputs, a subset of which contains a continuum of period-1 gaits forming a *semistable* set: perturbations off of any of its gaits result in transients that return to the set, though typically to different gaits.

1 Introduction

Humans are highly versatile bipedal walkers. Having learned as toddlers to take steps without falling, people can walk purposefully in a myriad of real-world situations. Successful walking requires, among other things, realizing an appropriate sequence of footsteps [1]. While walking, humans can perform goal-directed tasks, like staying on a path or walking alongside another person, with equal success via any one of infinitely many possible sequences of footsteps. Such task-level equifinality of foot placements, along with body-level biomechanical redundancies in muscles and joints [2], physiological motor noise [3], and environmental disturbances, all contribute to the significant variability observed in human walking [4–6]. Indeed, step-to-step observations of human walking provide a window into how the nervous system manages redundancies and equifinality while achieving task goals in specific walking contexts. However, the non-uniqueness of solutions

*Corresponding author: jpc3@psu.edu.

to any given walking task makes the modeling and analysis of such systems mathematically ill-posed.

We previously posited that humans achieve stable walking gaits via a hierarchical schema consisting of two functionally distinct sets of processes that we distinguish as *control* versus *regulation* [7]: whereas "control" refers to processes required for a walker to remain *viable*, i.e., to take steps without falling, "regulation" designates step-to-step processes a viable walker needs to carry out specific goal-directed *tasks*. The notion of viability [8] is well-suited to handle the ill-posedness of walking as it merely characterizes the walker's ability to avoid falls and is, therefore, agnostic to the existence of attracting steady states or goal-directedness. Conversely, by itself, regulation at the task level does not aim to ensure the walker's viability: on the contrary, it assumes viability as a prerequisite. The overall control architecture that results mirrors those obtained in engineered systems using *successive loop closure* [9, 10] with, in our case, the "control" subsystem responsible for viable stepping acting as the "inner loop" and the goal-directed "regulator" subsystem as the "outer loop". Moreover, its hierarchical structure is consistent with the neurophysiological architecture of perception-action processes responsible for human motor performance [11, 12].

People, particularly older adults, frequently fall while walking, and can experience serious injuries, such as hip fracture, especially after falling sideways [13, 14]. Taking wider steps can modify the lateral motion of the body's center of mass (CoM) to prevent such falls [1, 15, 16]. Thus, to reduce the incidence of falls, it is imperative to understand the dynamics of step-to-step foot placements in human walking, especially in the lateral direction. In previous experimental work [4–6], we used simple linear update models based on error minimization with respect to hypothesized walking task goals, or *motor regulation templates*, to study the variability structure of human stepping time series. Multiobjective models that strongly prioritized regulating step width over lateral body/CoM position replicated the fluctuation statistics of human lateral foot placements (figure 1). However, given that these empirical models are developed using only task-level stepping data, without consideration of underlying biomechanics, their effectiveness is, perhaps, surprising. It remains an open question how the Newtonian mechanics of the body, which is essentially nonlinear, can give rise to such linear regulation at the task level.

To address this question, we here couple a mechanical template [17, 18] for frontal plane stepping on level ground with an empirically verified motor regulation template [6]. The resulting *integrated template model* shows how motor regulation behavior observed in humans can indeed be obtained from mechanical first principles. We demonstrate that the apparent decoupling between dynamics at the task and body levels observed in experiments arises naturally from the hierarchical regulation scheme "embodied" in our model. Furthermore, we show how task-level optimal regulation creates a goal-equivalent manifold (GEM) [19] at the "body-level", i.e., in the system's extended state space of mechanical states and inputs.

Steady walking has commonly been thought of as a limit cycle, i.e., an asymptotically stable periodic gait [20, 21], possibly perturbed by noise [22, 23]. To remain versatile, however, humans have necessarily learned to walk with many periodic gaits, with different observables such as step length and step time, both stably and efficiently. Here, we find a manifold in the extended state space of the walker that is filled with periodic gaits, each of which is capable of achieving task-level goals. Furthermore, we show that at least a portion of this manifold forms a *semistable set* [24–27], i.e., a continuum of nonisolated periodic gaits such that perturbations off of any one of them result in transient dynamics that approach other, *typically different*, periodic gaits in the

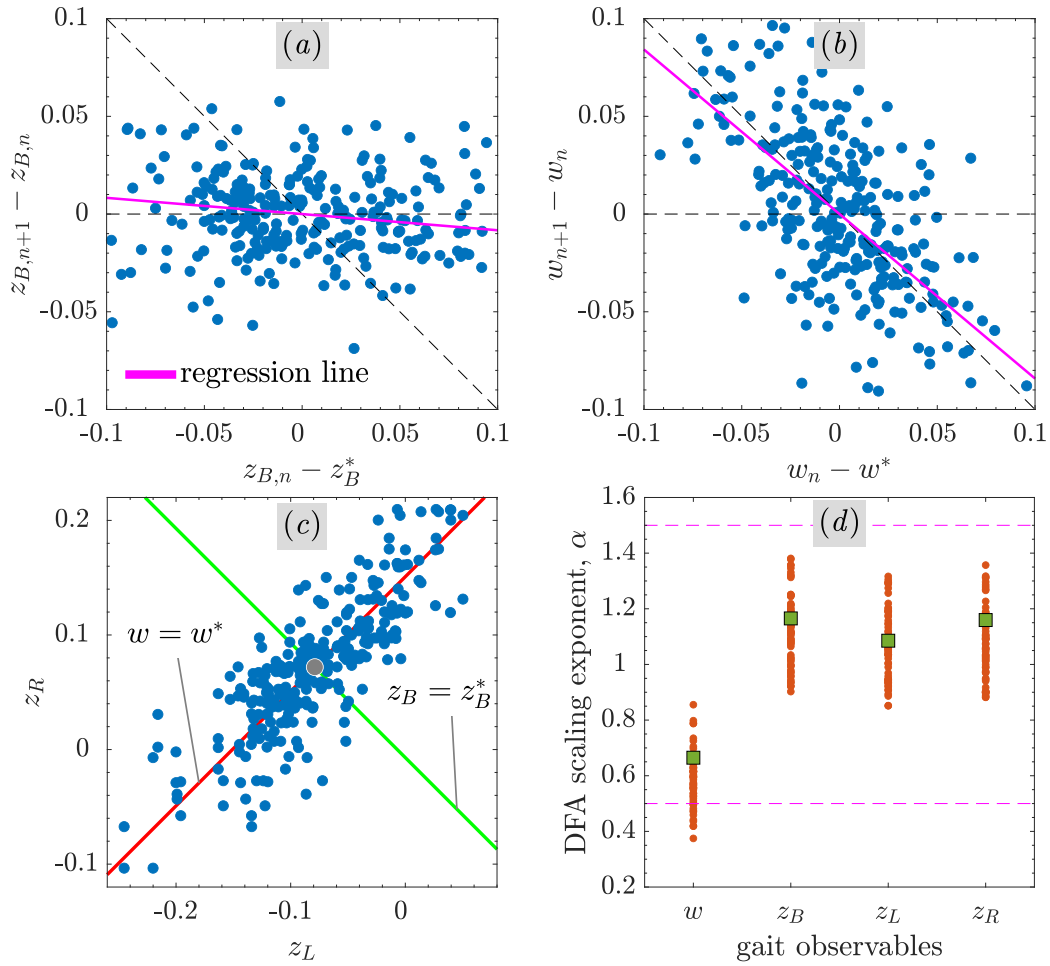

Figure 1 Human walking data showing step-to-step multiobjective regulation of lateral body position, z_B, and step width, w [6]. Typical experimental "direct control" plots [6] in (a) body position and (b) step width show how deviations from their respective target values (z_B^* and w^*) are corrected from one step to the next. Goals z_B^* and w^* are set to experimental averages $\overline{z}_B$ and $\overline{w}$, respectively. Linear regression shows that fluctuations in z_B are largely uncorrected (*regression line* slope ≈ 0); those in w are strongly corrected (slope ≈ -1). Same walking trial plotted in the stepping plane (c) of left and right foot placements (z_L, z_R) shows much larger fluctuations in z_B than w, where $z_B = \frac{1}{2}(z_R + z_L)$ and $w = z_R - z_L$. Only point at intersection (*filled circle*) of constant body position ($z_B = z_B^*$) and constant step width ($w = w^*$) goal equivalent manifolds (GEMs) perfectly satisfies both goals. Detrended fluctuation analysis (DFA) exponents, α, for different stepping observables (d): a fluctuation at step n is likely to be followed by a fluctuation at step $n+1$ of the same sign (i.e., it is persistent) if $\alpha > 0.5$; of opposite sign (i.e., antipersistent) if $0 < \alpha < 0.5$; $\alpha = 0.5$ for white noise, while $\alpha = 1.5$ for a pure random walk (*horizontal broken lines*). DFA α from a pooled data set (*dots*: 65 treadmill walking trials of 290 steps each; *filled squares*: sample trial in *a*-*c*) show much lower degree of statistical persistence in step width fluctuations than in body position and foot placements, consistent with the stronger regulation of w. Linear stochastic update models, or motor regulation templates, capture these statistical features of step-to-step fluctuations of observables $\{z_B, w\}$ (or, $\{z_L, z_R\}$). See [6] for detailed study.

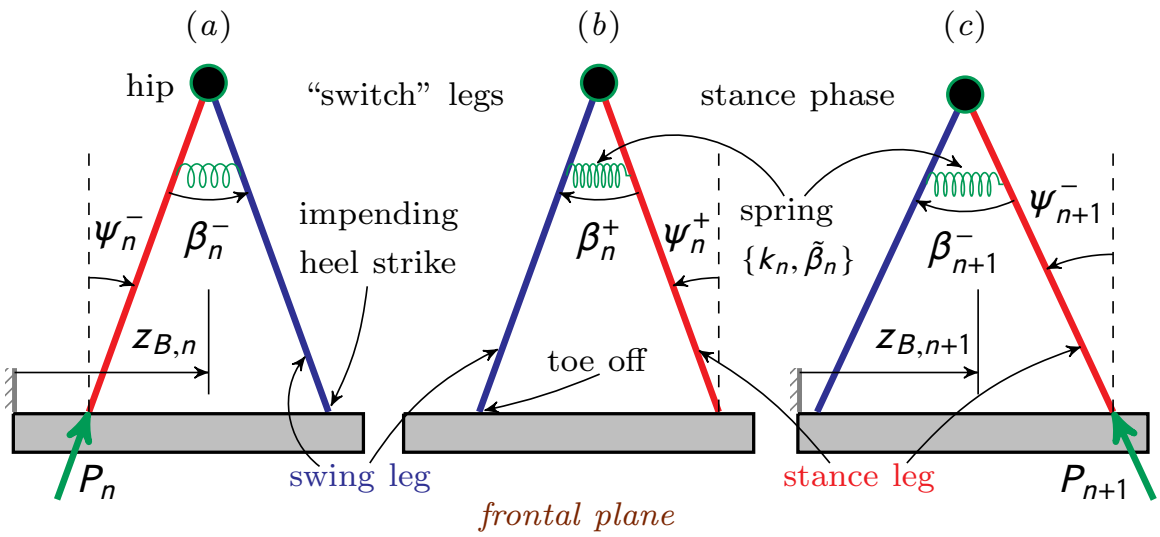

Figure 2 Three snapshots of a 2D powered compass walker with hip spring [18] adapted to walk laterally in the *frontal plane* on level ground: (*a*) just before n^{th}, (*b*) just after n^{th}, and (*c*) just before $(n+1)^{\text{st}}$ heel strike. The walker rocks back-and-forth in the frontal plane with anteroposterior axis directed into/out of the page. The walker has straight, massless, stance (*red*) and swing (*blue*) legs, and a point mass M at the hip (*circle*); point masses, m, at feet are infinitesimally small compared to M. Push-off impulse, P, is applied instantaneously just before heel strike (at which $\beta^- = 2\psi^-$) at the end of stance phase. Additional input parameters: torsional spring (*coil*) at hip, stiffness k and unstretched angle $\tilde{\beta}$, can be adjusted instantaneously at beginning of each stance phase. The walker's mechanical state in the lab frame just before applying P_n is $\mathbf{X}_n := [z_{B,n}, \psi_n^-, \dot{\psi}_n^-]^\top$ (see text).

set. The semistability of walking, demonstrated here for the first time, is a direct consequence of equifinality: it is less constraining than the asymptotic stability of limit cycles and is, therefore, more suitable to characterize stability of versatile biological walkers like humans. Moreover, semistability is consistent with the idea that humans can, at least in principle, remain viable (i.e., avoid falls) [8] by switching between regulation strategies and their corresponding steady-state periodic gaits [7].

2 Task-level regulation in the frontal plane

We adapt a 2D compass walker originally used to model sagittal-plane walking [18, 28] to study powered dynamics in the *frontal plane* on level ground (figure 2). The walker can adjust three input parameters $\{P, k, \tilde{\beta}\}$ at the beginning of each walking step: the impulsive push-off input $P \geqslant 0$ models ankle actuation during toe-off in humans; a linear torsional spring, with stiffness $k > 0$ and unstretched angle $\tilde{\beta} \geqslant 0$, models hip actuation during the stance phase [18, 29].

2.1 Discrete-time stepping dynamics

Every walking step begins with an instantaneous impulsive double-support phase (figure 2*a*-*b*) followed by a continuous-time single-support stance phase (figure 2*b*-*c*) so the walker's step-to-step dynamics are inherently *hybrid* [30].

The stance leg's mechanical state just before applying push-off P_n is $\mathbf{X}_n := [z_{B,n}, \psi_n^-, \dot{\psi}_n^-]^\top$, where z_B is the lateral body position in the inertial lab frame, ψ^- is the stance leg angle in the frontal plane, and $\dot{\psi}^-$ is its angular rate. The overall dynamics of the instantaneous double-support phase, consisting of push off, followed by a heel strike, and "switching" of stance and swing legs, is governed by the *impact map*:

$$\psi_n^+ = \psi_n^-, \tag{1a}$$
$$\dot{\psi}_n^+ = -\left[\dot{\psi}_n^- \cos 2\psi_n^- + P_n \sin 2\psi_n^-\right], \tag{1b}$$
$$\beta_n^+ = 2\psi_n^-, \tag{1c}$$
$$\dot{\beta}_n^+ = -\left(1 - \cos 2\psi_n^-\right)\left[\dot{\psi}_n^- \cos 2\psi_n^- + P_n \sin 2\psi_n^-\right] \tag{1d}$$

where the superscripts $-$ and $+$ indicate instants just before push off and just after heel strike, respectively. The walker's state just after n^{th} heel strike, $[z_{B,n}, \psi_n^+, \dot{\psi}_n^+]^\top$, is independent of its swing leg angular rate $\dot{\beta}_n^-$ just before push off (equation 1) [28]. Consequently, the stance leg's state $\mathbf{X}_n$ is, in fact, also the walker's state necessary to evolve its step-to-step dynamics forward in time.

During the nth continuous stance phase (figure 2), the walker's dynamics is governed by the ordinary differential equations (ODEs):

$$\ddot{\psi} = \sin\psi, \tag{2a}$$
$$\ddot{\beta} = \sin\psi - \sin\beta\left(\cos\psi - \dot{\psi}^2\right) - k_n(\beta - \tilde{\beta}_n), \tag{2b}$$

beginning from a state just after heel strike that lies on a codimension-two manifold Σ_n^+ in the above ODEs' 4D state space, and evolves to a state just before next push off that lies on a codimension-one Poincaré section Σ_{n+1}^-, where

$$\Sigma^+ \triangleq \left\{[\psi^+, \dot{\psi}^+, \beta^+, \dot{\beta}^+]^\top \mid \beta^+ = 2\psi^+, \dot{\beta}^+ = (1 - \cos 2\psi^+)\dot{\psi}^+\right\}, \tag{3a}$$
$$\Sigma^- \triangleq \left\{[\psi^-, \dot{\psi}^-, \beta^-, \dot{\beta}^-]^\top \mid \beta^- = 2\psi^-, \dot{\beta}^- < 2\dot{\psi}^-\right\}. \tag{3b}$$

The spring parameters $\{k_n, \tilde{\beta}_n\}$ remain fixed during the nth stance phase and do not affect the walker's discrete dynamics (equation 1) for massless legs with infinitesimally small feet (figure 2). The above equations of motion (equations 1-3) are expressed in nondimensionalized variables, viz., time $\tau := \sqrt{\frac{g}{l}}t$, impulse $P := \frac{P_i}{M\sqrt{gl}}$, stiffness $k := \frac{k_t}{mgl}$, where t, P_i, k_t are their dimensional counterparts, respectively, along with gravity g, leg length l, hip mass M, and foot mass m (figure 2).

Walking motion is feasible when $\psi^- \geqslant 0$, $\dot{\psi}^- \geqslant 0$, $\dot{\psi}^+ \leqslant 0$. The stance leg does not swing past vertical if

$$\dot{\psi}^+ \geqslant -2\sin\left(\frac{\psi^+}{2}\right), \tag{4}$$

thus precluding crossover steps. Consequently, we get an inequality constraint on the states and inputs (using equations 1 and 4):

$$\dot{\psi}^- \cos 2\psi^- + P \sin 2\psi^- \leqslant 2 \sin\left(\frac{\psi^-}{2}\right). \tag{5}$$

Using equation (1) and the solution to equation (2), the walker's step-to-step dynamics can be studied as a hybrid Poincaré map [30], $\mathbf{F}$, with state $\mathbf{X}_n := [z_{B,n}, \psi_n^-, \dot{\psi}_n^-]^\top$ and input parameter vector $\mathbf{u}_n := [P_n, k_n, \tilde{\beta}_n]^\top$ at step n:

$$\mathbf{X}_{n+1} = \mathbf{F}(\mathbf{X}_n, \mathbf{u}_n). \tag{6}$$

A period-1 gait (i.e., that repeats every step) corresponds to a fixed point $\mathbf{X}^* := [z_B^*, \psi^*, \dot{\psi}^*]^\top$ of the map $\mathbf{F}$ provided there is $\geqslant 1$ $\mathbf{u}^* := [P^*, k^*, \tilde{\beta}^*]^\top$ satisfying:

$$\mathbf{X}^* = \mathbf{F}(\mathbf{X}^*, \mathbf{u}^*). \tag{7}$$

For a given periodic body state $\mathbf{X}^*$ in the lab frame, there can be (infinitely) many input parameters $\mathbf{u}^*$, and vice versa. Thus, every period-1 gait $(\mathbf{X}^*, \mathbf{u}^*)$ is uniquely specified in the six-dimensional (6D) *extended* state space consisting of body states and inputs.

2.2 Lateral body position and step width regulation

We impose a multiobjective task-level stepping regulator [6] that aims to achieve an *a priori* fixed body position z_B^* and step width w^* simultaneously by choosing optimal lateral foot placement of the walker (figure 2) at each walking step. At the task level, the regulated observables $\{z_B, w\}$ are related to the "end effector" observables, i.e., foot placements $\{z_L, z_R\}$, as:

$$z_B = \frac{1}{2}\left(z_R + z_L\right), \tag{8a}$$

$$w = z_R - z_L, \tag{8b}$$

where $w \geqslant 0$, if there are no crossover steps.

The multiobjective regulation template selects the walker's next lateral foot placement as a weighted combination of two predicted foot placements, one that optimally achieves the step width goal $w = w^*$, and the other the body position goal $z_B = z_B^*$ [6]. Let the walker's right leg be its stance leg during step n (figure 2) so that

$$z_{R,n+1} = z_{R,n}. \tag{9}$$

Then, at the $(n+1)^{\text{st}}$ heel strike, the regulator places the walker's left foot laterally at $z_{L,n+1} = z_{L,n+1}^{\text{opt}}$, where

$$z_{L,n+1}^{\text{opt}} := \rho z_{L,n+1}^{\{w^*\}} + (1-\rho) z_{L,n+1}^{\{z_B^*\}}, \tag{10}$$

in which $z_{L,n+1}^{\{w^*\}}$ is the foot placement corresponding $w_{n+1} = w^*$ alone, $z_{L,n+1}^{\{z_B^*\}}$ is the foot placement corresponding $z_{B,n+1} = z_B^*$ alone, and the mixture parameter $\rho \in [0, 1]$ is kept fixed from step-to-step [6]: $\rho = 1$ corresponds to 100% w regulation and $\rho = 0$ to 100% z_B regulation. Using equations (8) and (9), we can write:

$$z_{L,n+1}^{\{w^*\}} = z_{R,n} - w^*, \tag{11a}$$

$$z_{L,n+1}^{\{z_B^*\}} = 2z_B^* - z_{R,n}, \tag{11b}$$

provided the walker can apply inputs that achieve the respective uniobjective targets w^* and z_B^* exactly. Substituting equations (11) in equation (10), we get the optimal left step as:

$$z_{L,n+1}^{\text{opt}} = (2\rho - 1)z_{R,n} - \rho w^* + 2(1-\rho)z_B^*. \tag{12}$$

The resulting weighted foot placement $z_{L,n+1}^{\text{opt}}$ (equations 10 and 12), in fact, minimizes the following task-level cost exactly:

$$C_{n+1}(z_{L,n+1}; z_{R,n}, \rho) := \rho[w_{n+1} - w^*]^2 + 4(1-\rho)[z_{B,n+1} - z_B^*]^2, \tag{13}$$

where w_{n+1} and $z_{B,n+1}$ are functions of $z_{L,n+1}$ (equation 8), and the optimal cost is (equations 11-13):

$$V_{n+1}(z_{R,n}; \rho) \triangleq \min_{z_{L,n+1}} C_{n+1}(z_{L,n+1}; z_{R,n}, \rho), \tag{14a}$$

$$= \rho(1-\rho)[2z_{R,n} - w^* - 2z_B^*]^2, \tag{14b}$$

$$= \rho(1-\rho)\left[z_{L,n+1}^{\{w^*\}} - z_{L,n+1}^{\{z_B^*\}}\right]^2. \tag{14c}$$

Similarly, for the left stance leg during step n, we obtain the walker's right foot placement at $z_{R,n+1} = z_{R,n+1}^{\text{opt}}$, where

$$z_{L,n+1} = z_{L,n}, \tag{15a}$$

$$z_{R,n+1}^{\text{opt}} = (2\rho - 1)z_{L,n} + \rho w^* + 2(1-\rho)z_B^*. \tag{15b}$$

Using equation (8) together with equations (9), (12), and (15), yields linear fluctuation dynamics of the task-level observables $\{z_B, w\}$ under multiobjective regulation:

$$\begin{bmatrix} z_{B,n+1} - z_B^* \\ w_{n+1} - w^* \end{bmatrix} = \mathbf{A} \begin{bmatrix} z_{B,n} - z_B^* \\ w_n - w^* \end{bmatrix}, \tag{16}$$

where

$$\mathbf{A} := \begin{cases} \begin{bmatrix} \rho & -\frac{\rho}{2} \\ -2(1-\rho) & 1-\rho \end{bmatrix} & \text{for the left stance leg,} \\ \\ \begin{bmatrix} \rho & \frac{\rho}{2} \\ 2(1-\rho) & 1-\rho \end{bmatrix} & \text{for the right stance leg.} \end{cases} \tag{17}$$

Since the matrix $\mathbf{A}$ only depends on ρ, linear task-level stepping dynamics (equation 16) is decoupled from body-level dynamics (equation 6) in the mechanical state space. However, the task-level observables $[z_B, w]^\top$ (or, $[z_L, z_R]^\top$) are nonlinear functions of the mechanical state and, moreover, the dynamics in the walker's state space itself is nonlinear.

Implicit in the successful realization of the task-level fluctuation dynamics (equation 16) is the requirement that the walker find valid inputs $\mathbf{u}_n$ for state $\mathbf{X}_n$ at each step (equation 6) so that the optimal foot placement can be achieved (equations 12 and 15b) or, equivalently, so that the global minimum of the multiobjective cost can be found (equations 13 and 14). We next show that not only is this possible, but also that the walker's body-level dynamics is, in a certain sense, stable under this multiobjective regulation.

3 Do task-level regulators yield stable body-level dynamics?

We first find period-1 gaits (equation 7) of the lateral walker consistent with task-level regulation. The targeted fixed point, $[z_B^*, w^*]^\top$, of the task-level dynamics (equation 16) directly determines two of the state variables, $z_B = z_B^*$ and $\psi^- = \psi^* := \arcsin\left(\frac{w^*}{2}\right)$ (figure 2), of any period-1 gait. Moreover, at the period-1 gaits, $\psi_n^+ = \psi_{n+1}^- = \psi^*$ (equation 1a) and, since the walker's stance phase is conservative (the energy $\frac{1}{2}\dot{\psi}^2 + \cos\psi$ = constant, via equation 2a), we have $\dot{\psi}_n^+ = -\dot{\psi}_{n+1}^- = -\dot{\psi}^*$, so that the push-off (equation 1b) satisfies:

$$P^* = \dot{\psi}^* \tan\psi^*. \tag{18}$$

Thus, for a given $\dot{\psi}^*$ (or P^*), one can obtain hip spring parameters $(k^*, \tilde{\beta}^*)$ that form a curve Γ in the $(k, \tilde{\beta})$-plane representing the locus of period-1 gaits, where

$$\Gamma \triangleq \left\{(k_n, \tilde{\beta}_n) \mid \psi_n^+ = \psi_{n+1}^- = \psi^* \;\Leftrightarrow\; \dot{\psi}_n^+ = -\dot{\psi}_{n+1}^- = -\dot{\psi}^* \;\forall n\right\}. \tag{19}$$

The set Γ is thus fully determined by $(\psi^*, \dot{\psi}^*)$ and is independent of the mixture parameter ρ (equation 10). Therefore, Γ yields the walker's period-1 gaits irrespective of the task-level regulation (equation 16) or lack thereof (as for the unregulated, open-loop walker). This fact demonstrates that the decoupling between task and body level fluctuation dynamics, identified in the previous section, extends to period-1 fixed points themselves.

To further examine the set of period-1 gaits, we carried out numerical analysis for the multiobjective goal $\{w^* \approx 0.12991, z_B^* \approx 0.06495\}$. This yields a 1D manifold, $\mathcal{M}_x$, of period-1 gaits (fixed points $\mathbf{X}^*$, equation 7), in the state space (figure 3*a*), along a line segment $\dot{\psi}^- = \dot{\psi}^* \in \left[0, \dot{\psi}_{\max}^*\right)$ with $z_B = z_B^*$, and $\psi^- = \psi^* := 0.065$, where the maximum angular rate (equations 4 and 5) is

$$\dot{\psi}_{\max}^* := 2\sin\left(\frac{\psi^*}{2}\right). \tag{20}$$

Correspondingly, we get a range of push-offs $P^* \in \left[0, \dot{\psi}_{\max}^* \tan\psi^*\right)$ from equation (18). We estimated curves Γ (equation 19) for each $\dot{\psi}^* \in \left[3.2494 \times 10^{-5}, 6.4924 \times 10^{-2}\right]$, with increments of $\Delta\dot{\psi}^* = 6.4989 \times 10^{-5}$, using a numerical continuation procedure. This yields the 2D manifold $\mathcal{M}_u$ corresponding to period-1 gaits in the region $\{(P, k, \tilde{\beta}) \in (0, 4.2302 \times 10^{-3}) \times (0, 12] \times [0.1, 0.26]\}$ of the input space (figure 3*b*).

3.1 Goal equivalent manifold of period-1 gaits

A hallmark of biological motor performance is *equifinality* [2], which states that a given goal-directed movement can be executed in many, typically an uncountable infinity of, ways. While this makes its mathematical formulation ill-posed, it is an essential feature of biological movement that makes it adaptive and resilient in the face of physiological noise, external disturbances, changing environmental conditions, and injuries.

Goal-directed movement tasks can be defined using a *goal function*, $\mathbf{g}$, of task-level observables (e.g., joint angles, or end effector positions and velocities) such that the zeros of $\mathbf{g}$ correspond to perfect task execution [19]. This set of task solutions defines a *goal equivalent manifold* (GEM), $\mathcal{G}$, in the space of observables [31, 32]. In experimental applications, the goal function is generally unknown *a priori* but is a testable hypothesis on the movement [4–6, 33]. Here we demonstrate

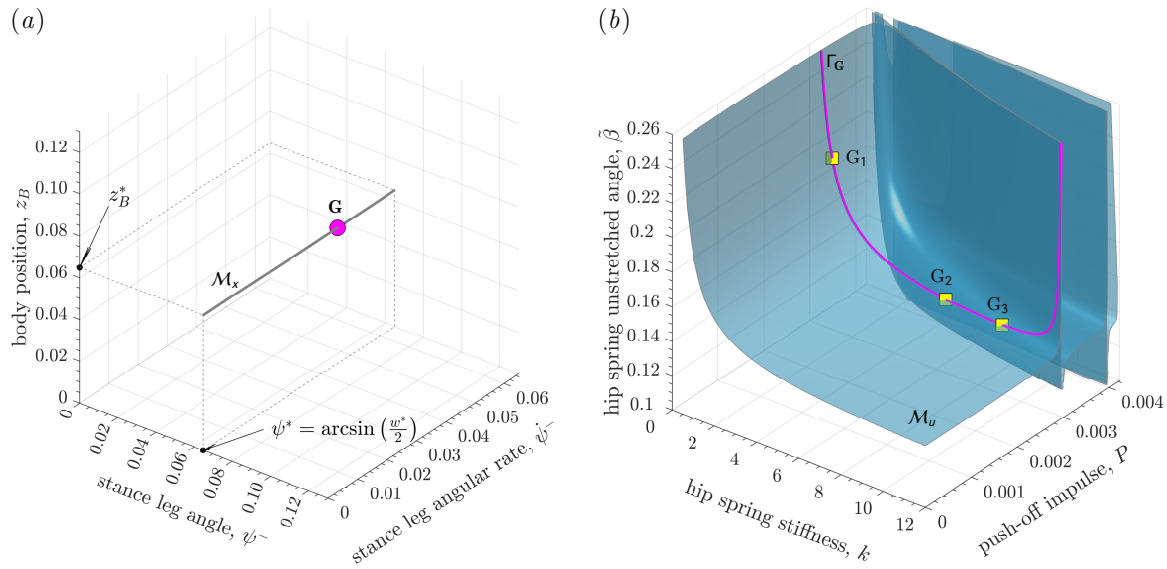

Figure 3 Period-1 gaits (equation 7) in the 6D extended state space comprised of (*a*) 3D mechanical state space and (*b*) 3D input space. For task-level multiobjective goal $\{w^* \approx 0.12991, z_B^* \approx 0.06495\}$, there is a 1D continuum of period-1 gaits with mechanical states on $\mathcal{M}_x$ at $\{z_B = z_B^*, \psi^- = \psi^* := 0.065\}$ ((*a*), *thick straight line segment*). For every point on $\mathcal{M}_x$ (e.g., point **G** at $\dot{\psi}^* \approx 0.045625$; *circle*) there is $\geqslant 1$ curve (equation 19) of inputs in the $(k, \tilde{\beta})$-plane (e.g, (*b*), $\Gamma_{\mathbf{G}}$ at $P^* = \dot{\psi}^* \tan \psi^* \approx 2.9698 \times 10^{-3}$; *thick curve*), each point on which yields a period-1 gait with same mechanical state. The points $\{G_1, G_2, G_3\} \in \Gamma_{\mathbf{G}}$ (*squares*) represent three such gaits. The collection of all such curves forms the manifold $\mathcal{M}_u$ (*b*). Thus, there is a 2D goal equivalent manifold $\mathcal{G}_{\mathrm{P1}}$ (equation 26) in the 6D extended state space, every point in which is a period-1 gait achieving $w = w^*$ and $z_B = z_B^*$.

theoretically that the GEM has a dual representation in the system's extended state space, which is the *combined* space of mechanical states *and* input parameters.

For lateral body position and step width regulation with goals $\{z_B^*, w^*\}$, respectively, the goal function is expressed most simply as

$$\mathbf{g}(z_B, w) := \left[z_B - z_B^*, w - w^*\right]^\top . \tag{21}$$

Thus, in the plane of task-level observables z_B and w, perfect execution of position and step width tasks are trivially specified by the lines $z_B = z_B^*$ and $w = w^*$, respectively, which define GEMs for position and step width goals *individually*. Using equations (8), these individual z_B and w GEMs get mapped to lines in the (z_L, z_R) stepping plane, used to display data from [6] in figure 1*c*. The z_B and w goals can be *simultaneously* achieved only at the point $(z_B, w) = (z_B^*, w^*)$. Here, we show how this "single point GEM" at the task level can be generated by the lateral walker.

We here assume that stepping regulation aims to achieve task-level goals $\{z_B^*, w^*\}$ exactly at the next step. We thus obtain a "1-step" GEM, $\mathcal{G}_1$, defined as:

$$\mathcal{G}_1 \triangleq \left\{ \left[\mathbf{X}_n{}^\top, \mathbf{u}_n{}^\top\right]^\top \,\middle|\, \mathbf{g}\left(z_{B,n+1}, w_{n+1}\right) = 0 \right\}, \tag{22}$$

where the goal function $\mathbf{g}$ is from equation (21), but its arguments $\{z_{B,n+1}, w_{n+1}\}$ are understood to be functions of the current extended state, $(\mathbf{X}_n, \mathbf{u}_n)$. The 2×6 Jacobian matrix of $\mathbf{g}\left(z_{B,n+1}, w_{n+1}\right)$, which maps small deviations in states and inputs to deviations at the task level [19], is then

$$\mathbf{J}_1 := \left[\frac{\partial \mathbf{g}\left(z_{B,n+1}, w_{n+1}\right)}{\partial \mathbf{X}_n} \quad \frac{\partial \mathbf{g}\left(z_{B,n+1}, w_{n+1}\right)}{\partial \mathbf{u}_n}\right]. \tag{23}$$

Generically, $\mathbf{J}_1$ has full rank (i.e., rank two) and, thus, the GEM $\mathcal{G}_1$ has co-dimension two, meaning that it is a 4D manifold in the 6D extended state space.

However, even when restricted to extended states $(\mathbf{X}, \mathbf{u})$ permitting a viable step [7], almost no points in $\mathcal{G}_1$ correspond to steady state gaits. Instead, under the dynamics of the system, extended states in $\mathcal{G}_1$ will evolve to whatever asymptotically stable gaits are permitted. Here, we focus on purposeful, steady walking, which we interpret as requiring that task-level goals be achieved via period-1 steady-state gaits. Thus, we define a "period-1" GEM, $\mathcal{G}_{\mathrm{P1}}$, as the subset of all state-input pairs in the GEM $\mathcal{G}_1$ (equation 22) that also yield period-1 gaits (equations 6 and 7):

$$\mathcal{G}_{\mathrm{P1}} \triangleq \left\{\left[\mathbf{X}_n{}^\top, \mathbf{u}_n{}^\top\right]^\top \,\middle|\, \mathbf{g}\left(z_{B,n+1}, w_{n+1}\right) = 0 \text{ and } \mathbf{X}_{n+1} - \mathbf{X}_n = 0\right\}. \tag{24}$$

Provided such period-1 gaits exist, the corresponding 5×6 Jacobian matrix,

$$\mathbf{J}_{\mathrm{P1}} := \left.\begin{bmatrix} \dfrac{\partial \mathbf{g}\left(z_{B,n+1}, w_{n+1}\right)}{\partial \mathbf{X}_n} & \dfrac{\partial \mathbf{g}\left(z_{B,n+1}, w_{n+1}\right)}{\partial \mathbf{u}_n} \\ \dfrac{\partial \mathbf{X}_{n+1}}{\partial \mathbf{X}_n} - \mathbf{I} & \dfrac{\partial \mathbf{X}_{n+1}}{\partial \mathbf{u}_n} \end{bmatrix}\right|_{\{\mathbf{X}_n=\mathbf{X}^*,\, \mathbf{u}_n=\mathbf{u}^*\}}, \tag{25}$$

where $\mathbf{I}$ is the identity matrix, generically has rank four. Thus, the GEM $\mathcal{G}_{\mathrm{P1}}$ has co-dimension four, so it is a 2D manifold in the extended state space. Equivalently, using the discussion surrounding equation (19), $\mathcal{G}_{\mathrm{P1}}$ can be defined by

$$\mathcal{G}_{\mathrm{P1}} \triangleq \left\{\left[\mathbf{X}^{*\top}, \mathbf{u}^{*\top}\right]^\top \,\middle|\, \mathbf{X}^* \in \mathcal{M}_x, \mathbf{u}^* \in \Gamma_{\mathbf{X}^*} \subset \mathcal{M}_u\right\}, \tag{26}$$

where $\Gamma_{\mathbf{X}^*}$ is the specific Γ curve of equation (19) (e.g., $\Gamma_{\mathbf{G}}$ in figure 3*b*) corresponding to the period-1 state $\mathbf{X}^*$ (point $\mathbf{G}$ in figure 3*a*). Indeed, the sub-manifolds $\mathcal{M}_x$ and $\mathcal{M}_u$ (figure 3) are the projections of the GEM $\mathcal{G}_{\mathrm{P1}}$ to the state and input space, respectively.

It is thus evident that there are uncountably many input parameters for any given period-1 gait that can equally achieve the task-level goal, as long as the walker remains viable [7]. That is, the lateral walker exhibits equifinality at the *body* level even though all such solutions are mapped into the point $(z_B, w) = (z_B^*, w^*)$ at the *task* level.

3.2 Implementing the multiobjective regulator

To implement optimal lateral foot placement (equations 12 and 15b) in code, we found it convenient to use the relationship of equation (8b) to optimize the step width:

$$w_{n+1}^{\mathrm{opt}} := \begin{cases} \rho w^* + 2(1-\rho)[z_B^* - z_{L,n}] & \text{for the left stance leg, and} \\ \rho w^* + 2(1-\rho)[z_{R,n} - z_B^*] & \text{for the right stance leg.} \end{cases} \tag{27}$$

In each of these cases, at step n the walker's regulator must select input parameters $\mathbf{u}_n = [P_n, k_n, \tilde{\beta}_n]^\top$ to pair with the current state $\mathbf{X}_n$ so that it can generate the next step. This is, again, mathematically ill-posed due to the existence of infinitely many solutions.

For our simulations, we set $\mathbf{u}_n$ to $\mathbf{u}_n^{\text{proj}}$, defined as the orthogonal projection of the walker's previously applied input, $\mathbf{u}_{n-1}$, onto the 2D target optimal-step-width manifold $\mathcal{M}_{u,n+1}$ in the input space corresponding to state $\mathbf{X}_n$:

$$\mathcal{M}_{u,n+1} := \left\{ \mathbf{u} \;\middle|\; \tilde{w}(\mathbf{u}; \mathbf{X}_n) = w_{n+1}^{\text{opt}} \right\}, \tag{28}$$

where $\tilde{w}$ is the step width considered as a function of the inputs with the current state $\mathbf{X}_n$ taken as a known parameter. In short, $\mathcal{M}_{u,n+1}$ is the set of all inputs guaranteeing that $w_{n+1} = w_{n+1}^{\text{opt}}$ (equations 27) at the next step; $\mathbf{u}_n^{\text{proj}} \in \mathcal{M}_{u,n+1}$ is a closest such input to $\mathbf{u}_{n-1}$. Note that, in general, $\mathcal{M}_{u,n+1} \not\subset \mathcal{M}_u$ (figure 3*b*) because $w_{n+1}^{\text{opt}} \neq w^*$. Given $\mathbf{X}_n$, $\mathbf{u}_n^{\text{proj}}$ was iteratively estimated until the magnitude of the smallest angle between the vector $\mathbf{u}_{n-1} - \mathbf{u}_n^{\text{proj}}$ and the normal to $\mathcal{M}_{u,n+1}$ at $\mathbf{u}_n^{\text{proj}}$ was less than 0.1°. This geometrical construction implies that our regulator implementation results in a step-to-step map acting on the space of state-input pairs, $(\mathbf{X}, \mathbf{u})$.

3.3 Semistability of the walker under multiobjective regulation

Task-level regulation does not in itself guarantee the existence of stable gaits. Thus, we first simulated the walker's trajectories with $\rho = 0.9$ (90% step width and 10% body position regulation; equations 10 and 13), as estimated in humans (figure 1;[6]). Typical trajectories of all six variables in the system's extended state space, starting from different initial states near a given period-1 gait, are shown in figure 4, in which two time scales are visible. In figure 4 (*left column, top two*), task-level regulation rapidly (in under 50 steps) drives z_B and ψ^- very close to their target values, thus placing the mechanical state, $\mathbf{X}$, nearly on $\mathcal{M}_x$ (figure 3*a*) and its extended state, $(\mathbf{X}, \mathbf{u})$, very close to the *targeted subset* of GEM $\mathcal{G}_1$ (equation 22), i.e., the portion of $\mathcal{G}_1$ on which $z_{B,n} = z_B^*$ and $\psi_n^- = \psi^*$ and, hence, the task-level goal function (equation 21) is $\mathbf{g} \approx 0$ for all subsequent steps.

However, at this point, the input $\mathbf{u}$ is not yet near $\mathcal{M}_u$ (figure 3*b*) and the system has yet to reach steady state. Further transients, particulary visible in the unregulated variables (figure 4 *left column, bottom* and *right column*), occur until trajectories settle (at about 500 steps) on period-1 gaits in GEM $\mathcal{G}_{\text{P1}}$ (equation 26), with different $\dot{\psi}^- \in \mathcal{M}_x$ and distinct steady state inputs in $\mathcal{M}_u$ (figure 3*b*). The latter stage of transients is an example of *self motion*, body-level dynamics that do not affect task-level performance [34, 35], consisting in this case of trajectories along the targeted subset of $\mathcal{G}_1$ that asymptotically approach the 2D $\mathcal{G}_{\text{P1}}$ while simultaneously satisfying task goals.

These numerical results demonstrate that at least a subset of $\mathcal{G}_{\text{P1}}$, the GEM containing period-1 gaits, is *semistable* [24–27]: trajectories starting from perturbations off of any gait in this set remain bounded and asymptotically return to other gaits embedded within it. A direct consequence of equifinality and the non-uniqueness of steady states, semistability is less constraining than the asymptotic stability of limit cycle walking. At least for disturbances in some neighborhood of $\mathcal{G}_{\text{P1}}$, the walker is guaranteed to return to a period-1 gait that, while typically different than the original, lies in the same GEM and so will achieve the same task goals. Indeed, using equation (14), one can show

$$V_{n+1} = (2\rho - 1)^2 V_n, \tag{29}$$

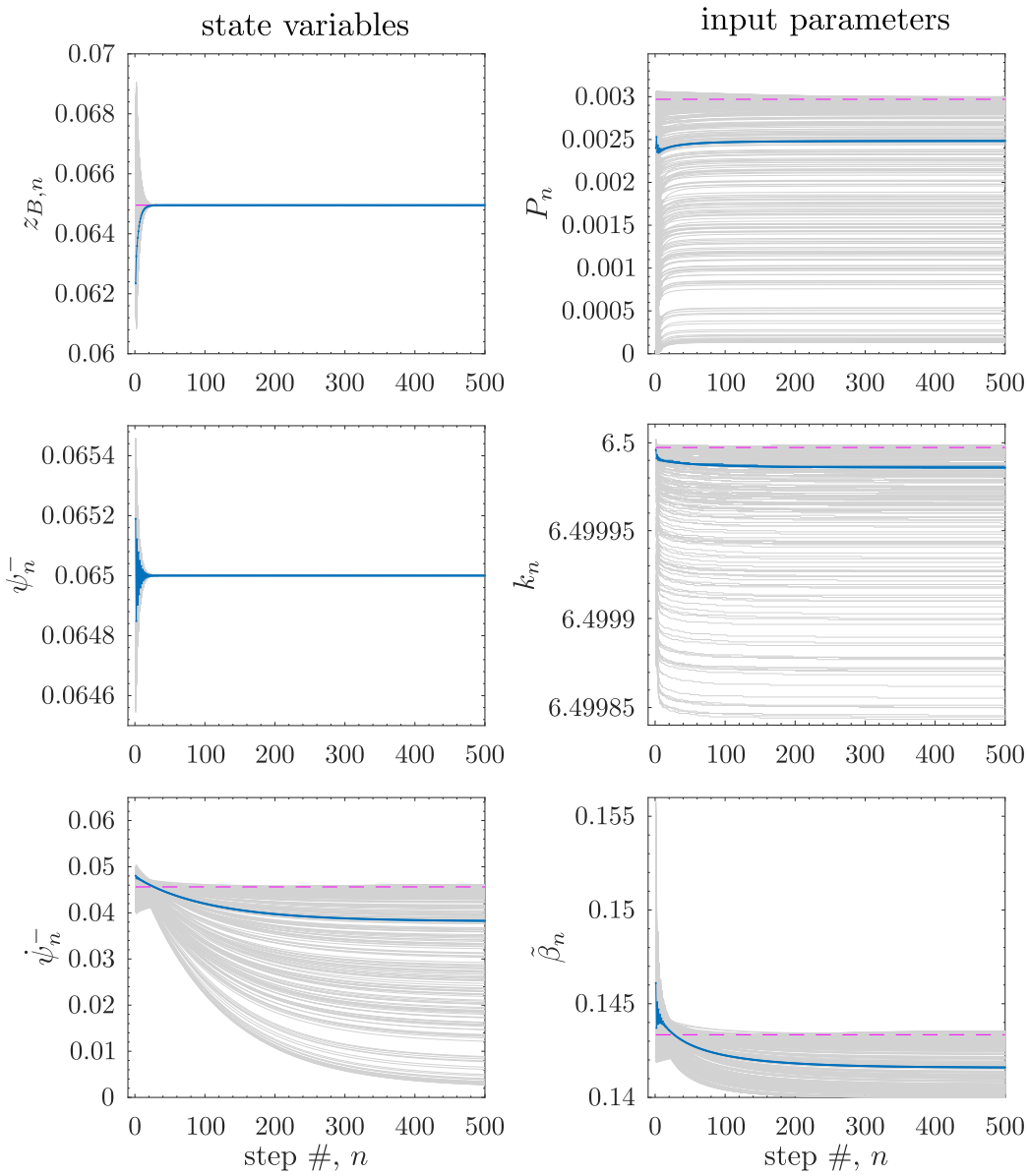

Figure 4 Semistable dynamics of period-1 gaits in the regulated system with $\rho = 0.9$: ensemble of time series (*thin gray curves*) of state, $\mathbf{X}$ (*left column*), and input, $\mathbf{u}$ (*right column*), starting from 475 distinct initial mechanical states $\mathbf{X}_1$ sampled uniformly randomly from surface of an ellipsoid around state $\mathbf{X} = \mathbf{G}$ (figure 3*a*): $\left(\frac{z_{B,1}}{z_B^*} - 1\right)^2 + \left(\frac{\psi_1^-}{\psi^*} - 1\right)^2 + \left(\frac{\dot{\psi}_1^-}{\dot{\psi}^*} - 1\right)^2 = 0.0025$. All trajectories used input $\mathbf{u}_0 = [P_0, k_0, \tilde{\beta}_0]^\top \approx [2.9698 \times 10^{-3}, 6.4999, 0.1433]^\top$ (*right column, broken horizontal lines*), point G_2 in figure 3*b*. Representative time series (*highlighted thick blue curve*) typifies semistability of regulated period-1 gaits: trajectories asymptotically approach distinct, Lyapunov stable period-1 gaits with mechanical states lying on $\mathcal{M}_x$ (figure 3*a*). Directly regulated state variables (*left column*, *top* and *middle*) rapidly approach their target values; the unregulated state variable (*left column*, *bottom*) more slowly approaches a point on $\mathcal{M}_x$, typically different from the reference point $\mathbf{G}$. At the same time, input trajectories (*right column*) approach distinct values on $\mathcal{M}_u$ (figure 3*b*), typically different from G_2.

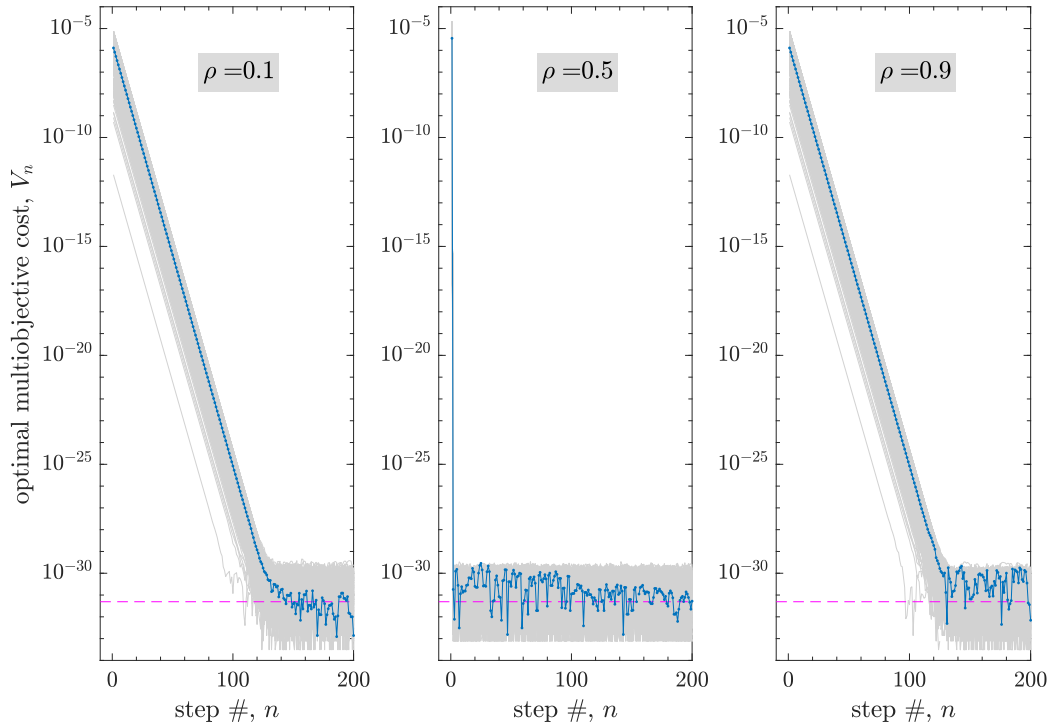

Figure 5 Monotonic decrease of the optimal multiobjective cost V_n (equation 14) along the task-regulated walker's deterministic trajectories initialized near gait G_2 (figure 3). For $\rho = 0.9$ stepping trajectories shown in figure 4. For $\rho \neq 0.5$, V_n hits a "noise floor" near ε^2 (*broken horizontal line*) after exponential decay ($\varepsilon \approx 2.204 \times 10^{-16}$, eps in MATLAB), with semilog slope $2 \ln |2\rho - 1|$ (from equation 29). This indicates an asymptotic approach to the targeted subset of GEM $\mathcal{G}_1$ (equation 22) that holds $z_{B,n} = z_B^*$ and $\psi_n^- = \psi^*$ (compare with figure 4, *left column, top two*). For $\rho = 0.5$, $V_n = 0$ (within numerical precision) in two steps, indicating finite-time convergence. Irrespective of ρ, trajectories asymptotically approach the semistable GEM $\mathcal{G}_{\mathrm{P1}}$ of period-1 gaits (equation 26).

so the minimized cost V_n evaluated along trajectories (as, e.g., in figure 4) decreases monotonically for $0 < \rho < 1$ (figure 5). Thus, V_n, defined in terms of task-level observables that themselves are functions of the walker's state, behaves like a *Lyapunov function* [24–27] with respect to the targeted subset of $\mathcal{G}_1$ (equation 22). This is consistent with the semistability of the walker's period-1 gaits on the attracting submanifold $\mathcal{G}_{\mathrm{P1}} \subset \mathcal{G}_1$ (equation 26).

3.4 Lateral walker with motor noise: fluctuation dynamics

To compare the integrated template's lateral stepping dynamics with human data, we simulated the system with "motor" noise, modeled as independent Gaussian noise of amplitude σ_m on the input at step n:

$$\mathbf{u}_n = \left[\, \mathbf{I} + \sigma_m \mathrm{diag}(\boldsymbol{\nu}_n) \right] \mathbf{u}_n^{\mathrm{proj}}, \tag{30}$$

where $\mathbf{u}_n^{\text{proj}}$ (equation 28 and surrounding discussion) is the deterministically optimal input, $\mathbf{I}$ is the identity matrix, $\boldsymbol{\nu}_n$ is a vector of standard normal random variables, and $\text{diag}(\boldsymbol{\nu}_n)$ is a diagonal matrix with principal diagonal $\boldsymbol{\nu}_n$.

With the mixture parameter again set to $\rho = 0.9$, the stochastically perturbed walker with 1% Gaussian motor noise ($\sigma_m = 0.01$) was able to walk (i.e., to remain viable [7] for) at least 500 steps. Ensembles of time series obtained from 475 stochastic simulations, all starting from the same period-1 gait, are shown in figure 6. Deviations in the regulated variables, ψ^- and z_B, both display significant diffusion, but relatively low drift: instead, they oscillate closely around their target values (recall that $w = 2\sin\psi^-$). Fluctuations in both variables appear to settle into a stochastic steady state after roughly 200 steps. However, steady-state ψ^- fluctuations have visibly smaller temporal correlations (i.e., their random oscillations are much more rapid) than those of z_B: as discussed in more detail below, this arises from the much stronger weight ($\rho = 0.9$) given to w regulation in these simulations.

In contrast, the time series ensembles for $\dot{\psi}^-$, P, k, and $\tilde{\beta}$, which are not directly regulated, display both diffusion and drift. The drift is an example of *stochastic* self motion along $\mathcal{G}_1$, during which, in contrast, the regulated variables fluctuate with approximately zero mean about their targeted values. Thus, the mechanical state drifts primarily in $\dot{\psi}^-$, i.e., along the manifold $\mathcal{M}_x$ (figure 3*a*), consistent with the semistability of the deterministic walker (figure 4), as it settles on a stochastic steady state near a new period-1 gait. The drifting behavior is a stochastic transient that lasts for hundreds of steps, longer than required to achieve approximate steady state at the task level (variables ψ^- and z_B). One finds that, again consistent with semistability, the steady-state probability distributions of these drifting variables depend on their initialization in the extended state space (figure 3; equation 26).

The temporal correlation differences observed in the plots of ψ^- and z_B (figure 6) can be quantified using detrended fluctuation analysis (DFA; [36–38]), which yields the scaling exponent α: $\alpha > 0.5$ indicates statistical *persistence*, meaning that a fluctuation at one step is likely to be followed by a fluctuation of the same sign at the next step, whereas $0 < \alpha < 0.5$ indicates *anti*persistence, so fluctuations at sequential steps are likely to alternate in sign; $\alpha = 0.5$ for uncorrelated noise and $\alpha \geqslant 1.5$ for unbounded random walks.

In experiments with human participants [4, 5, 33, 39–43], the DFA exponent provides a signature of motor regulation: tightly regulated task-level variables tend to have $\alpha \approx 0.5$, whereas unregulated variables have $0.5 \ll \alpha < 1.5$. This "tightness-of-control interpretation" [43] of DFA suggests an hypothesis on the organization of the human motor regulation system that is, however, difficult (if not impossible) to study only through experiments. Even the most clever of experimental protocols have limited access to internal parameters of the neuromotor and biomechanical systems responsible for movement and, even when there is such access, the relevant parameters cannot typically be adjusted.

We thus estimated α for noisy time series simulated with different values of the mixture parameter ρ to see if its effect on the fluctuation properties of the observables $\{w, z_B, z_L, z_R\}$ conformed with the tightness-of-control hypothesis. Recall these observables are not independent (equations 8) and the regulator explicitly minimizes costs in w and z_B, weighted by ρ (equation 13). For $\rho = 0.9$ (figure 7 *right*), the strongly regulated variable, w, has $\alpha[w] \approx 0.5$, whereas the weakly regulated z_B has much higher values ($\alpha[z_B] \approx 1$). Furthermore, the lower persistence of w relative to z_B ($\alpha[w] \ll \alpha[z_B]$) quantifies the apparent lower temporal correlation of w with respect to z_B, visible in the time series of figure 6 (*left column, top two*). In contrast, the

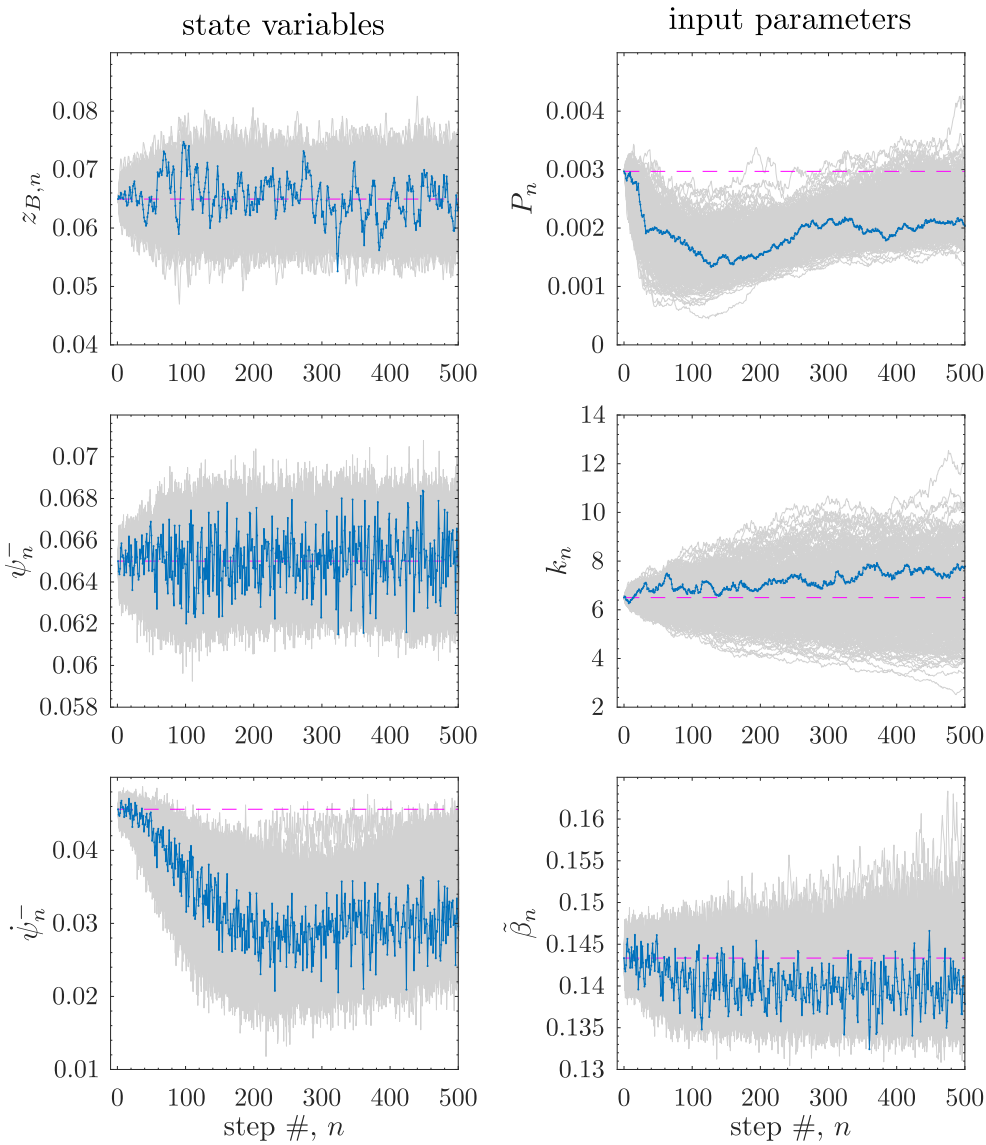

Figure 6 Lateral walker with simulated motor noise: ensembles (*thin gray curves*) of state (*left column*) and input (*right column*) time series with $\sigma_m = 1\%$ Gaussian noise (equation 30) added to optimal inputs at each step, with $\rho = 0.9$. Initial conditions (*broken horizontal lines*) corresponded to gait G_2 (figure 3); 475 stochastic realizations (time series) were generated using distinct seeds to a pseudorandom number generator. A representative time series (*highlighted thick blue curve*) demonstrates typical behavior under stochastic perturbations: mechanical state trajectories are regulated transverse to the GEM and so oscillate close to $\mathcal{M}_x$ (figure 3*a*) after a diffusive transient (*left column, top* and *middle*); however, there is drift away from the initial period-1 orbit along $\mathcal{M}_x$ (*left column, bottom*) and in the input space (*right column*; also see $\mathcal{M}_u$, figure 3*b*). The set of period-1 gaits on the GEM on which trajectories settle (say, at step 500) with high probability depends on initial conditions. Consistent with 90% w regulation ($\rho = 0.9$), ψ^- time series (given $w = 2\sin\psi^-$) shows significantly less persistence of fluctuations compared to z_B (also see figure 7).

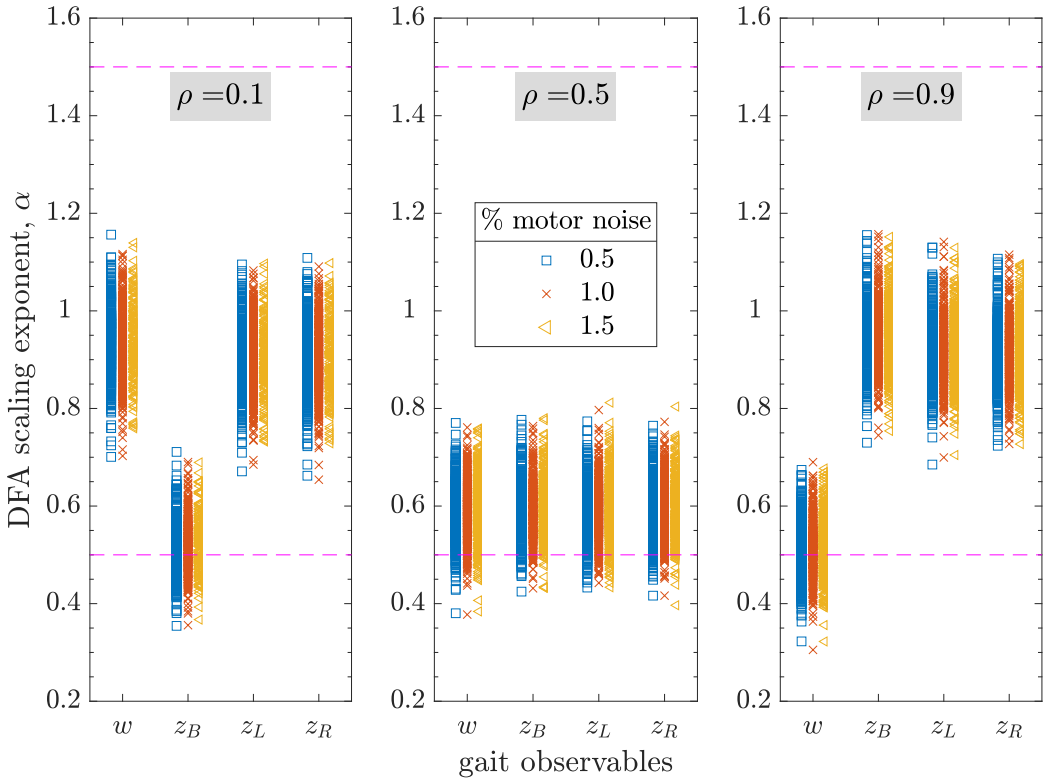

Figure 7 Detrended Fluctuation Analysis (DFA) results for the regulated walker with simulated motor noise and mixture parameter $\rho \in \{0.1, 0.5, 0.9\}$. We computed scaling exponents α (*markers*) for noisy time series (475 trials; 500 steps per trial) of stepping observables $\{w, z_B, z_L, z_R\}$ at three motor noise levels $\sigma_m \in \{0.5, 1, 1.5\}$%: for reference, $\alpha = 0.5$ for white noise and $\alpha = 1.5$ for a Brownian random walk (*broken lines*). All time series were initialized at gait G_2 (figure 3), as in figure 6 for $\rho = 0.9$. Consistent with the "tightness-of-control interpretation" of α, fluctuations in step width become more persistent ($\alpha[w]$ increases) and those in the body position become less persistent ($\alpha[z_B]$ decreases) as the degree of step width regulation ρ decreases from 0.9 to 0.1. Fluctuations in all observables show uniformly low persistence when both w and z_B are regulated to the same degree ($\rho = 0.5$). Humans walking on a treadmill choose their lateral foot placements in a way that resembles multiobjective regulation with $\rho \approx 0.9$ ([6]; figure 1*d*). Note that DFA α is not significantly affected by noise strength σ_m.

individual step positions, z_L and z_R, which are not directly regulated, have high persistence, with DFA exponents comparable to $\alpha[z_B]$. Taken together, these results closely mirror those found in experiments with walking humans (figure 1*d*).

Figure 7 (*left*) shows the corresponding DFA results for $\rho = 0.1$. Here, the relative degree of persistence swaps between the two variables: for z_B, which is strongly regulated, $\alpha[z_B] \approx 0.5$, whereas $\alpha[w] \approx 1$. Finally, when both variables are equally regulated ($\rho = 0.5$, figure 7 *center*), the persistence of fluctuations is comparably low for all the variables. These simulation results support the tightness-of-control hypothesis: as the regulation shifts from predominantly weighting w to z_B, the DFA α for both undergoes a corresponding shift, as predicted. The uniformity of α

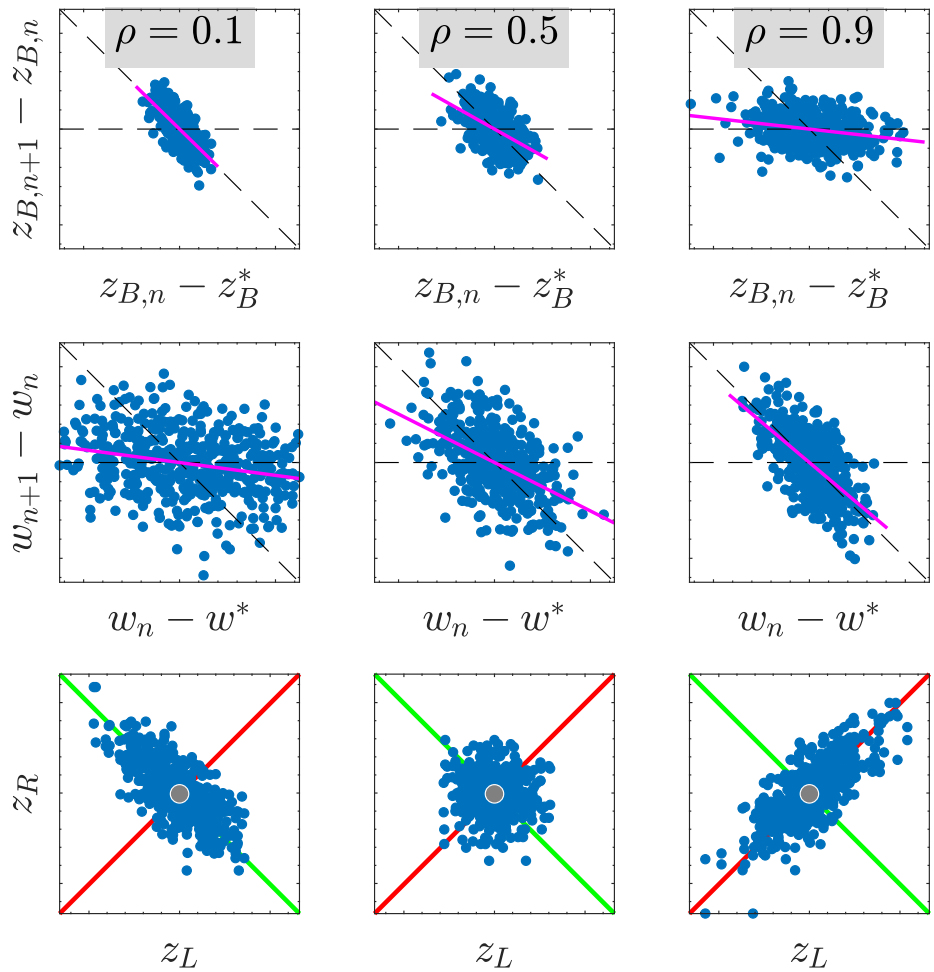

Figure 8 Typical step-to-step fluctuation data (*dots*) of lateral body position (z_B), step width (w), and foot placements (z_L, z_R) of the stochastically perturbed (1% motor noise) regulated walker for $\rho \in \{0.1, 0.5, 0.9\}$. Compare each *column* (at a given ρ) to a typical experimental trial in human walking (figure 1*a-c*). As the degree of step width regulation ρ decreases, the persistence of step-to-step fluctuations in z_B also decreases (*regression line* slope changes from ≈ 0 to ≈ -1; *top row*), while that in w increases (*regression line* slope changes from ≈ -1 to ≈ 0, *middle row*). Same walking trial plotted in the stepping plane (*bottom row*) shows increase in fluctuations in z_B and simultaneous decrease in fluctuations in w as ρ increases: *data ellipse* is oriented along $z_B = z_B^*$ (*green line*) for $\rho < 0.5$ and along $w = w^*$ (*red line*) for $\rho > 0.5$. At $\rho = 0.5$, the variability structure of foot placements is isotropic. The stepping fluctuation dynamics and the variability structure for $\rho = 0.9$ (*right column*) resembles that observed in human data (figure 1*a-c*).

values across all variables when $\rho = 0.5$ is a new observation, but not completely unexpected, as discussed below.

Typical scatter plots of stepping data from the stochastically perturbed walker are shown in figure 8, in which columns correspond to simulations with $\rho \in \{0.1, 0.5, 0.9\}$. The top two

rows in each column present "direct control" analyses ([6]; figure 1*a,b*) of the simulated data: for perfect regulation, meaning that a deviation from the target value is, on average, eliminated at the next step, the regression line in such plots would have slope -1.

In the right-most column of figure 8, for which $\rho = 0.9$, we see that the direct control plot for w indeed has a regression slope ≈ -1, whereas the slope for the z_B is near zero. This is entirely as expected, given that in this case w and z_B are strongly and weakly regulated, respectively. Importantly, these results are consistent with the DFA results of figure 7 (*right*) for the same value of the mixture parameter. Furthermore these simulation results again mirror those obtained in experiments with human participants (figure 1*a,b*).

Varying ρ in our simulations gives results that similarly cohere with the DFA analyses of figure 7: in figure 8 (*top row*), as ρ varies from 0.1 to 0.9, the regression slope for the z_B direct control plots changes from ≈ -1 to ≈ 0, while the slope for the w plots (figure 8 *middle row*) exhibits the opposite change. Thus, DFA and direct control analyses provide complementary and consistent characterizations of regulation strength.

The bottom row of figure 8 displays stepping data in the (z_L, z_R) plane. As in the experimental plot of figure 1*c*, lines are included indicating task-level GEMs for $w = w^*$ and $z_B = z_B^*$, individually; the combined "GEM" for the multiobjective task is the point at their intersection. In all cases, we observe that principal axes of the data ellipses are approximately aligned with the single-variable lines, and the sample mean is near the intersection point. For $\rho = 0.9$, the major axis of the ellipse lies along the w GEM, as expected: strong w regulation minimizes the distance of steps from this line, whereas weak z_B regulation permits steps to spread along it. When $\rho = 0.1$, the strength of regulation reverses, and stepping data aligns with the z_B GEM.

When w and z_B are regulated to the same degree, at $\rho = 0.5$, the data ellipse (figure 8 *bottom row*, *center*) is close to a circle. This phenomenon has been observed in experiments in which people were asked to change lanes while walking [44, 45]: during steady walking before and after the lane change, stepping data conformed with the w-dominated $\rho \approx 0.9$ case of figure 8 (*bottom row, right*; and as in figure 1*c*), whereas during the transition step, scatter plots were closer to circles, suggesting that participants regulated w and z_B nearly equally. This isotropy of the simulated stepping plane data when $\rho = 0.5$ provides a geometrical counterpoint to the DFA of the same gait observables for the same value of ρ (figure 7, *center*).

We conclude this section with a caveat. Here, we can interpret DFA from first principles: we know what variables are being regulated as parameters are varied, and so can show how this regulation correlates with estimates of α. However, care must be taken when using DFA exponents to make inferences about motor regulation strength from experimental data because completely passive, open loop aspects of a system impact DFA. It can easily be shown that α is functionally related to the local stability properties of a given steady state [31], whether or not the system is feedback controlled. Thus, while the tightness-of-control hypothesis says that if a particular variable is tightly regulated, then $\alpha \approx 0.5$, the converse need not be true. For this reason, tightness-of-control interpretations of experimental DFA results need to be grounded in the analysis of data from task-level variables with a plausible need for motor regulation and should, whenever possible, be checked against results for other variables and under conditions that might change such regulation. Finally, the resulting assessments should be checked against other empirical measures of correlation as well.

4 Discussion and conclusions

We introduced a simple lateral dynamic walker, with swing leg dynamics and three adjustable input parameters, to study how motor regulation affects frontal plane stepping (figure 2). The walker's adjustable push off provides between-step actuation; its adjustable hip spring tunes within-step swing dynamics. Motivated by experimental observations and phenomenological models of human stepping regulation [6], we imposed task-level multiobjective regulation targeting the walker's optimal lateral foot placement at each step. The regulator prioritizes achieving a step width, vis-à-vis the walker's lateral body position, to varying degrees by choosing a mixture parameter ρ. Our model thus integrated a lateral *mechanical template* [17], which captures fundamental mechanics of frontal-plane walking, with a lateral *motor regulation template* [6], an empirically verified model of how humans manipulate lateral foot placements in a goal-directed manner.

Our system provides a physically grounded example of the hierarchical control schema hypothesized in experiments [4–6, 19, 31–33, 44], in which an inner "control" loop responsible for movement execution serves as the plant for an outer "regulation" loop used to accurately achieve movement goals. In engineering, such cascaded architectures typify applications of *successive loop closure* (SLC) [9, 10], a design approach used in automation and robotics including, most relevantly here, autonomous vehicles [46–48]. SLC provides a useful framework for conceptualizing human movement on multiple grounds. First, the neurophysiology of the motor system possesses a similar hierarchical structure [11, 12], with an "inner" subsystem responsible for movement execution and an "outer" subsystem responsible for motor planning and coordination (see, e.g., [11, figure 4]). Second, SLC lends itself to the incremental development of cascaded models that, in principle, span all levels from "neurons to whole-body motion" [17]. A given integrated template might be "anchored" by further physiological and/or biomechanical inner loops: e.g., the hip spring in the template studied here might be "unpacked" into an inner loop involving reflex-mediated muscle groups. Likewise, outer loops might be added representing perceptual/cognitive processes needed, e.g., for navigation and obstacle avoidance. Finally, SLC conceptually parallels biological motor skill acquisition in which new motor capabilities are developed by exploiting previously learned, more basic abilities (e.g., children first learn to crawl, then stand, then walk, then run [49]).

Experiments with human participants tested this general schema using hypotheses on error-correcting regulation at the task level, meaning, for walking, with respect to goals specified solely by stepping observables. This paper provides the first demonstration that such task-level regulation can arise from a physics-based dynamic walking system and, in turn, resolves two outstanding theoretical challenges. Arguably the most fundamental of such challenges concerns how empirical multiobjective linear models, in stepping observables alone, can so effectively capture observed stepping dynamics (e.g., [6], figure 1). This may seem surprising given that, not only is the underlying biomechanical system undoubtedly nonlinear, but such models are estimated without reference to the walker's mechanical state, thereby seeming to "ignore Newtonian dynamics". However, our integrated template model precisely achieves this condition: the multiobjective regulator design yields linear step-to-step dynamics at the task level that are decoupled from the walker's body-level nonlinear dynamics (see equations 16, 17, and 19 and surrounding discussion).

Motor variability and regulation in the presence of equifinality [2] has only been studied experimentally using goal equivalent manifolds (GEMs) [19, 31] defined in the space of task-level observables [4, 6, 33]. Thus, a second challenge concerns how goal equivalence at the task level,

which is directly observable in experiments, is reflected at the body level, which is not. Here, we demonstrated that the body-level GEM is a manifold in the system's *extended state space* (the combined space of mechanical states and inputs). Our system has 3D mechanical state and input parameter vectors (section 2.1), giving a 6D extended state space. For an optimal stepping regulator specifying only target values of step width and lateral position, we obtained a 4D GEM, $\mathcal{G}_1$ (equation 22) in the extended state space. However, most points in $\mathcal{G}_1$ are not steady state gaits: we showed that the dynamics of the regulated system drives extended states onto $\mathcal{G}_{\mathrm{P1}}$ (equation 26), a 2D submanifold of $\mathcal{G}_1$, that contains a continuum of period-1 gaits all satisfying stepping goals and, hence, is also a GEM.

We studied the dynamics in the extended state space by simulating the walker's trajectories with $\rho = 0.9$ (90% step width and 10% body position regulation), consistent with models of lateral stepping regulation in humans (figure 1; [6]). We found that at least a subset of the GEM containing the walker's period-1 gaits is *semistable* [24–27]. That is, if the system is perturbed away from any of the continuum of goal-equivalent period-1 gaits in $\mathcal{G}_{\mathrm{P1}}$, the transient behavior attracts the state back to $\mathcal{G}_{\mathrm{P1}}$, but typically to a *different* period-1 gait. Thus, while the *individual* solutions are not asymptotically stable, at least a portion of the GEM *is*. Indeed, the walker's minimized multiobjective cost at each step (equation 14a) behaves like a Lyapunov function (equation 29; [27]), demonstrating the asymptotic stability of the targeted subset of $\mathcal{G}_1$ on which the task goals are satisfied for all steps, and which itself contains $\mathcal{G}_{\mathrm{P1}}$. This suggests semistability can be expected to be a property of systems with "GEM aware" optimal regulators of the type studied here.

Simulations of the walker with motor noise showed that the walker can remain viable [7] for several hundred steps, displaying stepping fluctuation statistics closely mirroring those observed in humans. Results were consistent with the "tightness of control" interpretation of the DFA exponent, α [43]: fluctuations in step width become more persistent, as quantified by α, and those in body position become less persistent as ρ decreases from 0.9 to 0.1. The degree of persistence in the task-level observables at $\rho = 0.9$ (figure 7) matches well with that observed in human experiments (figure 1*d*). Moreover, the walker's step-to-step fluctuation dynamics and task-level variability structure for $\rho = 0.9$ (figure 8, *right column*) resembles that observed in human data (figure 1*a*-*c*). Step-to-step foot placements show least persistence and a nearly isotropic variability structure when $\rho = 0.5$ (i.e., with the same degree of step width and body position regulation), a phenomenon observed as people take transition steps during lane change maneuvers [44, 45]. Finally, even though the step-to-step task-level dynamics are strongly regulated, the walker's stochastic trajectories at the body level show significant drift and diffusion of the mechanical states and inputs, consistent with the minimum intervention principle [50, 51] and the phenomenon of self motion [34, 35].

We found that semistable walking relative to a goal equivalent manifold of gait solutions was a natural consequence of task-level optimal regulation. Semistable walking is a less constraining paradigm than that provided by asymptotically stable limit cycles and, therefore, is more suitable for biological walking, which is characterized by its flexibility and adaptability. Moreover, semistability is consistent with the idea that humans can, at least in principle, remain viable (i.e., avoid falls) by rapidly switching between regulation strategies and corresponding goal-equivalent sets of steady-state gaits [7]. Supported by our results, and the knowledge that equifinality is commonplace in human movement, we propose that optimal task-level regulation provides a conceptualization of walking as arising from an already-learned collection of viable stepping solutions between which

humans can switch at each step by, e.g., changing task goals and/or cost functions. This allows for highly adaptive gaits that enable walkers to quickly and effectively respond to changing task requirements, environmental conditions, and external disturbances.

References

[1] Sjoerd M. Bruijn and Jaap H. van Dieën. Control of human gait stability through foot placement. *J. R. Soc. Interface*, 15(143):20170816, 2018. doi:10.1098/rsif.2017.0816.

[2] Nikolai Aleksandrovich Bernstein. *The co-ordination and regulation of movements*. Pergamon Press, Oxford, 1967.

[3] A. Aldo Faisal, Luc P. J. Selen, and Daniel M. Wolpert. Noise in the nervous system. *Nat. Rev. Neurosci.*, 9(4):292–303, 2008. ISSN 1471-0048. doi:10.1038/nrn2258.

[4] Jonathan B. Dingwell, Joby John, and Joseph P. Cusumano. Do humans optimally exploit redundancy to control step variability in walking? *PLoS Comput. Biol.*, 6(7):e1000856, 2010. doi:10.1371/journal.pcbi.1000856.

[5] Jonathan B. Dingwell and Joseph P. Cusumano. Identifying stride-to-stride control strategies in human treadmill walking. *PLOS ONE*, 10(4):e0124879, 2015. doi:10.1371/journal.pone.0124879.

[6] Jonathan B. Dingwell and Joseph P. Cusumano. Humans use multi-objective control to regulate lateral foot placement when walking. *PLoS Comput. Biol.*, 15(3):1–28, 2019. doi:10.1371/journal.pcbi.1006850.

[7] Navendu S. Patil, Jonathan B. Dingwell, and Joseph P. Cusumano. Viability, task switching, and fall avoidance of the simplest dynamic walker. *Sci. Rep.*, 12(1):8993, 2022. doi:10.1038/s41598-022-11966-3.

[8] Jean-Pierre Aubin. *Viability Theory*. Birkhäuser, Boston, MA, 2009. doi:10.1007/978-0-8176-4910-4.

[9] M.C. Berg, N. Amit, and J.D. Powell. Multirate digital control system design. *IEEE Trans. Autom. Control*, 33(12):1139–1150, 1988. ISSN 1558-2523. doi:10.1109/9.14436.

[10] Sigurd Skogestad and Ian Postlethwaite. *Multivariable Feedback Control: Analysis and Design*. John Wiley & Sons, 2005. Google-Books-ID: 97iAEAAAQBAJ.

[11] Trevor Drew and Daniel S Marigold. Taking the next step: cortical contributions to the control of locomotion. *Curr. Opin. Neurobiol.*, 33:25–33, 2015. ISSN 0959-4388. doi:10.1016/j.conb.2015.01.011.

[12] Guy A. Orban, Alessia Sepe, and Luca Bonini. Parietal maps of visual signals for bodily action planning. *Brain Struct. Funct.*, 226(9):2967–2988, 2021. ISSN 1863-2661. doi:10.1007/s00429-021-02378-6.

[13] J. Parkkari, P. Kannus, M. Palvanen, A. Natri, J. Vainio, H. Aho, I. Vuori, and M. Järvinen. Majority of hip fractures occur as a result of a fall and impact on the greater trochanter of the femur: A prospective controlled hip fracture study with 206 consecutive patients. *Calcif. Tissue Int.*, 65(3):183–187, 1999. doi:10.1007/s002239900679.

[14] Elizabeth R. Burns, Judy A. Stevens, and Robin Lee. The direct costs of fatal and non-fatal falls among older adults — united states. *J. Saf. Res.*, 58:99–103, 2016. doi:10.1016/j.jsr.2016.05.001.

[15] Colum D. MacKinnon and David A. Winter. Control of whole body balance in the frontal plane during human walking. *J. Biomech.*, 26(6):633–644, 1993. doi:10.1016/0021-9290(93)90027-c.

[16] Catherine E. Bauby and Arthur D. Kuo. Active control of lateral balance in human walking. *J. Biomech.*, 33(11):1433–1440, 2000. doi:10.1016/s0021-9290(00)00101-9.

[17] R.J. Full and D.E. Koditschek. Templates and anchors: neuromechanical hypotheses of legged locomotion on land. *J. Exp. Biol.*, 202(23):3325–3332, 1999.

[18] Arthur D. Kuo. Energetics of Actively Powered Locomotion Using the Simplest Walking Model. *J. Biomech. Eng.*, 124(1):113–120, 2001. ISSN 0148-0731. doi:10.1115/1.1427703.

[19] Joseph P. Cusumano and Paola Cesari. Body-goal variability mapping in an aiming task. *Biol. Cybern.*, 94(5):367–379, 2006. doi:10.1007/s00422-006-0052-1.

[20] Daan G.E. Hobbelen and Martijn Wisse. Limit cycle walking. In Matthias Hackel, editor, *Humanoid Robots, Human-like Machines*, chapter 14. IntechOpen, Rijeka, 2007. doi:10.5772/4808.

[21] Tad McGeer. Passive Dynamic Walking. *Int. J. Rob. Res.*, 9(2):62–82, 1990. doi:10.1177/027836499000900206.

[22] Katie Byl and Russ Tedrake. Metastable Walking Machines. *The International Journal of Robotics Research*, 28(8):1040–1064, 2009. ISSN 0278-3649. doi:10.1177/0278364909340446.

[23] Jimmy Li-Shin Su and Jonathan B. Dingwell. Dynamic Stability of Passive Dynamic Walking on an Irregular Surface. *J. Biomech. Eng.*, 129(6):802–810, 2007. ISSN 0148-0731. doi:10.1115/1.2800760.

[24] Bernd Aulbach. *Continuous and Discrete Dynamics near Manifolds of Equilibria*. Springer-Verlag, Berlin Heidelberg, 1984. doi:10.1007/bfb0071569.

[25] D. S. Bernstein and S. P. Bhat. Lyapunov stability, semistability, and asymptotic stability of matrix second-order systems. *J. Mech. Design*, 117(B):145–153, 1995. doi:10.1115/1.2836448.

[26] S.P. Bhat and D.S. Bernstein. Lyapunov analysis of semistability. In *Proceedings of the 1999 American Control Conference*, volume 3, pages 1608–1612, 1999. doi:10.1109/ACC.1999.786101.

[27] Wassim M. Haddad, Junsoo Lee, and Sanjay P. Bhat. Asymptotic and finite-time semistability for nonlinear discrete-time systems with application to network consensus. *IEEE Transactions on Automatic Control*, 68(2):766–781, 2023. doi:10.1109/TAC.2022.3142189.

[28] Mariano Garcia, Anindya Chatterjee, Andy Ruina, and Michael Coleman. The Simplest Walking Model: Stability, Complexity, and Scaling. *J. Biomech. Eng.*, 120(2):281–288, 1998. doi:10.1115/1.2798313.

[29] Bradford L. Rankin, Stephanie K. Buffo, and Jesse C. Dean. A neuromechanical strategy for mediolateral foot placement in walking humans. *J. Neurophysiol.*, 112(2):374–383, 2014. doi:10.1152/jn.00138.2014.

[30] Navendu S. Patil, Jonathan B. Dingwell, and Joseph P. Cusumano. Task-level regulation enhances global stability of the simplest dynamic walker. *J. R. Soc. Interface*, 17(168): 20200278, 2020. doi:10.1098/rsif.2020.0278.

[31] Joseph P. Cusumano and Jonathan B. Dingwell. Movement variability near goal equivalent manifolds: Fluctuations, control, and model-based analysis. *Hum. Movement Sci.*, 32(5): 899–923, 2013. doi:10.1016/j.humov.2013.07.019.

[32] Joseph P. Cusumano, Joseph M. Mahoney, and Jonathan B. Dingwell. The dynamical analysis of inter-trial fluctuations near goal equivalent manifolds. In Mindy F. Levin, editor, *Progress in Motor Control*, volume 826 of *Advances in Experimental Medicine and Biology.*, pages 125–145, New York, NY, 2014. Springer. doi:10.1007/978-1-4939-1338-1_9.

[33] Joby John, Jonathan B. Dingwell, and Joseph P. Cusumano. Error correction and the structure of inter-trial fluctuations in a redundant movement task. *PLOS Comput. Biol.*, 12 (9):e1005118, 2016. doi:10.1371/journal.pcbi.1005118.

[34] V. Martin, J. P. Scholz, and G. Schöner. Redundancy, Self-Motion, and Motor Control. *Neural Comput.*, 21(5):1371–1414, 2009. ISSN 0899-7667. doi:10.1162/neco.2008.01-08-698.

[35] John P. Scholz and Gregor Schöner. Use of the uncontrolled manifold (UCM) approach to understand motor variability, motor equivalence, and self-motion. In Mindy F. Levin, editor, *Progress in Motor Control*, volume 826 of *Advances in Experimental Medicine and Biology*, pages 91–100, New York, NY, 2014. Springer. doi:10.1007/978-1-4939-1338-1_7.

[36] C.-K. Peng, S. V. Buldyrev, S. Havlin, M. Simons, H. E. Stanley, and A. L. Goldberger. Mosaic organization of DNA nucleotides. *Phys. Rev. E*, 49:1685–1689, 1994. doi:10.1103/PhysRevE.49.1685.

[37] J. M. Hausdorff, C. K. Peng, Z. Ladin, J. Y. Wei, and A. L. Goldberger. Is walking a random walk? evidence for long-range correlations in stride interval of human gait. *J. Appl. Physiol.*, 78(1):349–358, 1995. doi:10.1152/jappl.1995.78.1.349.

[38] Ary L. Goldberger, Luis A. N. Amaral, Jeffrey M. Hausdorff, Plamen Ch. Ivanov, C.-K. Peng, and H. Eugene Stanley. Fractal dynamics in physiology: Alterations with disease and aging. *Proc. Natl. Acad. Sci.*, 99(suppl_1):2466–2472, 2002. doi:10.1073/pnas.012579499.

[39] Jonathan B. Dingwell and Joseph P. Cusumano. Re-interpreting detrended fluctuation analyses of stride-to-stride variability in human walking. *Gait Posture*, 32(3):348–353, 2010. doi:10.1016/j.gaitpost.2010.06.004.

[40] Philippe Terrier and Olivier Dériaz. Persistent and anti-persistent pattern in stride-to-stride variability of treadmill walking: Influence of rhythmic auditory cueing. *Hum. Movement Sci.*, 31(6):1585–1597, 2012. doi:https://doi.org/10.1016/j.humov.2012.05.004.

[41] Melvyn Roerdink, Andreas Daffertshofer, Vivien Marmelat, and Peter J. Beek. How to sync to the beat of a persistent fractal metronome without falling off the treadmill? *PLOS ONE*, 10(7):1–13, 2015. doi:10.1371/journal.pone.0134148.

[42] Philippe Terrier. Fractal fluctuations in human walking: Comparison between auditory and visually guided stepping. *Ann. Biomed. Eng.*, 44(9):2785–2793, 2016. doi:10.1007/s10439-016-1573-y.

[43] Melvyn Roerdink, Christa P. de Jonge, Lisette M. Smid, and Andreas Daffertshofer. Tightening up the control of treadmill walking: Effects of maneuverability range and acoustic pacing on stride-to-stride fluctuations. *Front. Physiol.*, 10, 2019. doi:10.3389/fphys.2019.00257.

[44] David M. Desmet, Joseph P. Cusumano, and Jonathan B. Dingwell. Adaptive multi-objective control explains how humans make lateral maneuvers while walking. *PLOS Comput. Biol.*, 18(11):1–27, 2022. doi:10.1371/journal.pcbi.1010035.

[45] David M. Desmet, Meghan E. Kazanski, Joseph P. Cusumano, and Jonathan B. Dingwell. How healthy older adults enact lateral maneuvers while walking. *Gait Posture*, 108:117–123, 2024. doi:https://doi.org/10.1016/j.gaitpost.2023.11.020.

[46] Randal W. Beard and Timothy W. McLain. *Small Unmanned Aircraft: Theory and Practice*. Princeton University Press, 2012.

[47] Adnan Saeed, Ahmad Younes, Shafiqul Islam, Jorge Dias, Lakmal Seneviratne, and Guowei Cai. A review on the platform design, dynamic modeling and control of hybrid uavs. In *2015 International Conference on Unmanned Aircraft Systems (ICUAS) Denver Marriott Tech Center Denver, Colorado, USA, June 9-12, 2015*. IEEE, 2015.

[48] Murillo Ferreira Dos Santos, Accacio Ferreira Dos Santos Neto, Leonardo De Mello Honório, Mathaus Ferreira Da Silva, and Paolo Mercorelli. Robust and Optimal Control Designed for Autonomous Surface Vessel Prototypes. *IEEE Access*, 11:9597–9612, 2023. ISSN 2169-3536. doi:10.1109/ACCESS.2023.3239591.

[49] Karen E. Adolph, Whitney G. Cole, Meghana Komati, Jessie S. Garciaguirre, Daryaneh Badaly, Jesse M. Lingeman, Gladys L. Y. Chan, and Rachel B. Sotsky. How do you learn to walk? Thousands of steps and dozens of falls per day. *Psychol. Sci.*, 23(11):1387–1394, 2012. doi:10.1177/0956797612446346.

[50] Emanuel Todorov. Optimality principles in sensorimotor control. *Nat. Neurosci.*, 7(9): 907–915, 2004. doi:10.1038/nn1309.

[51] Emanuel Todorov and Michael I. Jordan. Optimal feedback control as a theory of motor coordination. *Nat. Neurosci.*, 5(11):1226–1235, 2002. doi:10.1038/nn963.